Available online at www.sciencedirect.com
ScienceDirect
Journal of Nuclear Materials 374 (2008) 185–191
journal of nuclear materials
www.elsevier.com/locate/jnucmat

Corrosion of Alloy 690 process pot by sulfate containing high level radioactive waste at feed stage

P. Sengupta [a,*], N. Soudamini [a,b], C.P. Kaushik [a,b], Jagannath [a,c], R.K. Mishra [a,b], G.B. Kale [a], K. Raj [a,b], D. Das [a,d], B.P. Sharma [a,e]

[a] Materials Science Division, Bhabha Atomic Research Centre, Mumbai 400 085, India
[b] Waste Management Division, Bhabha Atomic Research Centre, Mumbai 400 085, India
[c] Technical Physics and Prototype Engineering Division, Bhabha Atomic Research Centre, Mumbai 400 085, India
[d] Chemistry Division, Bhabha Atomic Research Centre, Mumbai 400 085, India
[e] Chemical Engineering Group, Bhabha Atomic Research Centre, Mumbai 400 085, India

Received 10 February 2007; accepted 15 August 2007

Abstract

Prolonged exposure of Alloy 690 process pot to sulfate containing high level radioactive waste leads to (a) depletion of Cr from the alloy, (b) intergranular attack and (c) building up of Cr_2O_3–Ni_2O_3–Fe_2O_3 mixed oxide surface layer containing Na and Cs sulfate precipitates. Time dependence of material loss from Alloy 690 is found to follow a linear relationship of the type Δw (material loss) $= -7.05 + 0.05t$. Corrosion rate calculated for 2400 h exposure is 3.66 mpy. Cr and Ni leach rates obtained for the same sample are 1.61 g m^{-2} d^{-1} and 2.52 g m^{-2} d^{-1}, respectively. Ni leach rates followed a linear time dependence relationship of the type dNL_{Ni}/dt (leach rate) $= -0.09 + 0.027t$, whereas Cr leach rates obeyed a non-linear relationship of the type dNL_{Cr}/dt (leach rate) $= 0.241 + 0.027t - 1.33 \times 10^{-4}t^{1/2}$.

PACS: 81.65.kn; 21.65.+f; 81.05.kf

1. Introduction

Durability assessment of melter pot materials used for vitrification of nuclear high level liquid waste (HLW) is an integral part for its life estimation studies. Recently, Bhabha Atomic Research Centre (BARC) has undertaken an initiative to understand hot walled induction melter pot materials performance under service conditions. Such melter pots are currently being used at Waste Immobilization Plant (WIP), Trombay, BARC to condition its sulfate containing HLW in indigenously developed sodium barium borosilicate matrix in batch-wise manner [1]. The melter pot design is based on multiple containment concepts where the actual vitrification process takes place in Alloy 690 process pots, surrounded by Alloy 690 susceptor and thermal insulator. To this process pot, nitric acid-based (1–3 M HNO_3) sulfate containing HLW and glass additive slurry are charged through different channels [2]. The entire vitrification process, including multiple stages, e.g. feed stage, i.e. mixing of HLW and glass additive slurry, evaporation, calcination, melt formation and soaking at different temperatures, is done in the same process pot (Table 1). Each of the process stages involves multiple chemical reactions that make the environment within process pot extremely corrosive. As in plant scale HLW-vitrification is done in a batch-wise manner, so cyclic operations of each of these stages make the scenario even worse. To circumvent this problem many countries, e.g. France and United Kingdom, have segmented the vitrification process into two parts [3]. In this segmented process flow-sheet, in the first stage, liquid HLW is fed separately into rotary calciner

* Corresponding author. Tel.: +91 22 2559 0468.
E-mail address: sengupta@barc.gov.in (P. Sengupta).

0022-3115/$ - see front matter © 2007 Elsevier B.V. All rights reserved.
doi:10.1016/j.jnucmat.2007.08.005

Table 1
Temperature schedules followed for HLW-vitrification

Stage/process	Process pot temperature (°C)
Feeding	100–105
Evaporation	105–120
Calcination	300–700
Fusion and melt formation	700–850
Soaking	900–950
Pouring	950–1000

for its calcination. In the next stage, the calcined mass is fed to process pot together with glass forming additives, and the mixture is heated in a stepwise manner to prepare borosilicate melt following the vitrification stages narrated above. Adoption of a two-stage process for immobilization of HLW is found to be successful as it could increase the life of process pot significantly. The issue that becomes apparent from the success of the two-stage process is that interaction between Alloy 690 process pot and HLW plays a crucial role in deciding the durability of melter pot. Unfortunately, this aspect has not received its due attention from scientific community engaged in waste management. The present paper focuses on this aspect and describes the mode of interaction between Alloy 690 process pot and sulfate containing HLW at feed stage.

2. Experimental procedure

2.1. Sample preparation

Commercially available mill annealed Alloy 690 sheet used for fabricating process pot has been used for the present study. Coupons of 20 mm × 8 mm × 5 mm dimension were cut from Alloy 690 plate, metallographically polished to 1 μm finish and drilled on one side. To avoid handling of radioactive materials during experiments, simulated HLW was used in place of actual BARC-HLW. Composition of the simulated HLW is given in Table 2. For the present experiment, coupons were dipped completely within hot (100 °C) simulated HLW (80 ml) using Teflon wire (Fig. 1). The solution was kept in a 250 ml round-bottomed flask provided with an air cooled condenser of length 1.5 m to prevent the loss of solution. The experiments were carried out for different time intervals (96–2400 h) and at the end of each experiment the coupon was removed, dried and weighed.

Table 2
Compositions of simulated HLW used in the present study

Component	Concentration (g/l)
$Ca(NO_3)_3 \cdot 4H_2O$	22.42
$Al(NO_3)_3 \cdot 9H_2O$	88.92
$Fe(NO_3)_3 \cdot 9H_2O$	42.42
$NaNO_3$	105.79
$Ni(NO_3)_2 \cdot 6H_2O$	3.65
CrO_3	1.11
UO_3 powder	22.3
$CsNO_3$	0.18
$Sr(NO_3)_2$	0.04
Na_2SO_4	14.72
$Ce(NO_3)_2 \cdot 6H_2O$	0.02
Nd_2O_3	0.01
RuO_2	0.01
Molarity	1.25 M

2.2. Analytical procedures

Surface and cross-sectional analyses of exposed coupons and unexposed coupons (as blank) were carried out using electron probe micro-analyzer (EPMA) and X-ray photoelectron spectroscopy (XPS). Inductively coupled plasma-atomic emission spectroscopy was used for liquid analysis. Brief notes on these analytical techniques are given below.

2.2.1. Analysis of the coupons

EPMA analyses of exposed and unexposed coupons were done using CAMECA SX-100. For surface layer characterization, exposed coupons were not polished and were studied as it is. For cross-sectional studies, exposed samples were mounted in resin and their cross-sections were ground with emery paper and subsequently polished with diamond paste of 1 μm grain size. An acceleration voltage of 20 keV and stabilized beam current of 4 nA and 20 nA were used for 'back scattered electron (BSE)' imaging and qualitative/quantitative analysis, respectively. The beam size was kept at $\leqslant$1 μm to reduce the convolution effect so as to arrive at good compositional estimates.

X-ray photoelectron spectroscopy (XPS) analyses were carried out for all exposed coupons and one unexposed as-received mill annealed sample using Mg Kα X-ray (1253.6 eV) primary radiation source. The binding energies were calibrated with respect to the Au $4f_{7/2}$ peak occurring at 84 eV.

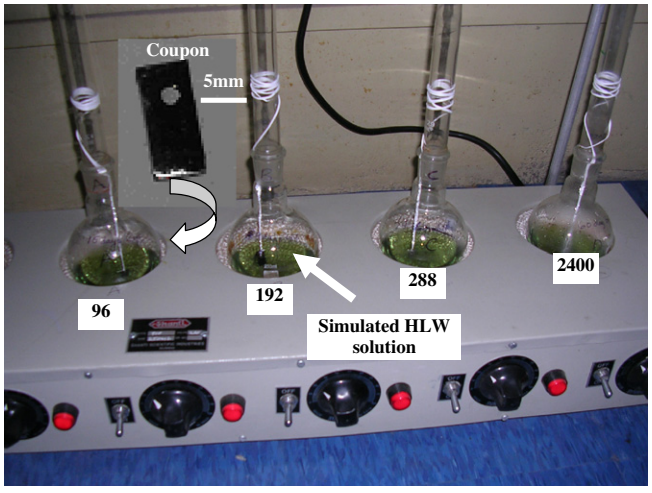

Fig. 1. Experimental set-up used in the present study. Numerical digits refer to time durations (in h) of Alloy 690/simulated HLW interactions. A representative Alloy 690 coupon is also shown in the inset.

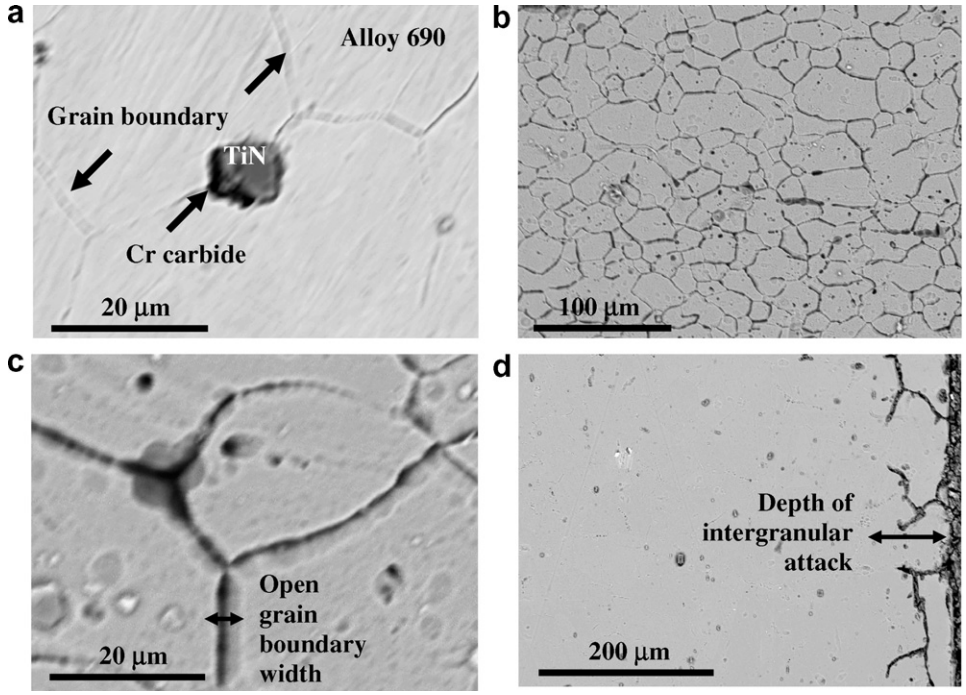

Fig. 2. BSE images showing representative microstructures of (a) as-received mill annealed Alloy 690 coupon, (b)–(c) surficial microstructure of coupon treated with simulated waste for 384 h (under different magnifications) and (d) cross-section of the same coupon showing the depth of intergranular attack.

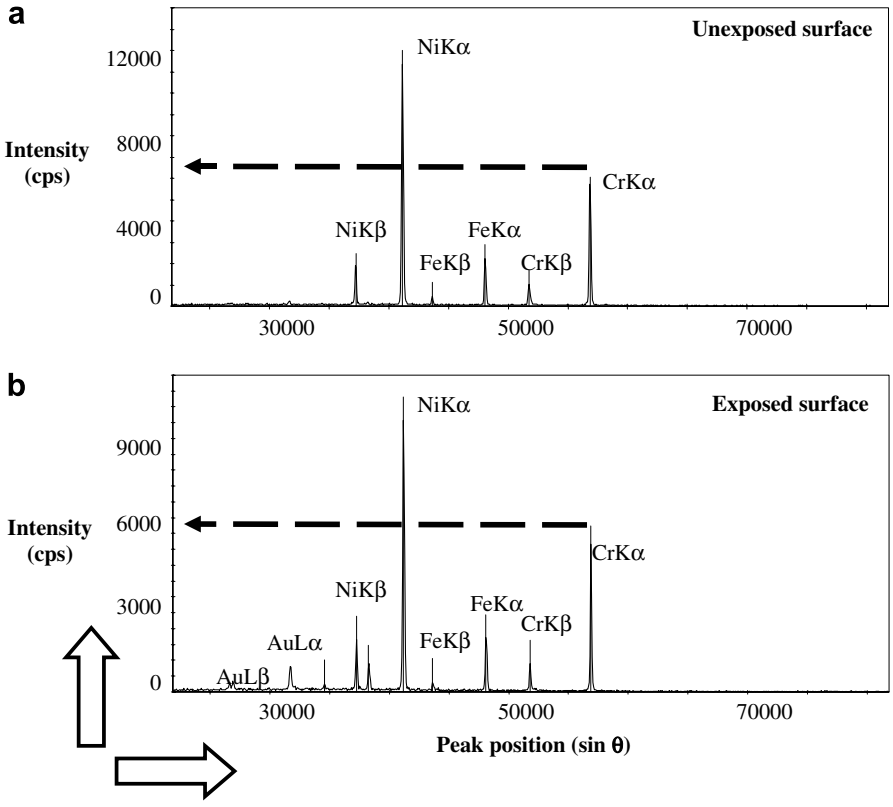

Fig. 3. X-ray spectrums (LIF crystal) showing the variations in Ni, Cr and Fe X-ray intensities at grain boundaries between (a) unexposed and (b) exposed surfaces of the coupon treated with simulated waste for 384 h (x-axis values indicate sin θ values multiplied by 10^6 for better X-ray peak separation).

2.2.2. Analysis of leachates

Leachates obtained from each of these experiments were analyzed by inductively coupled plasma-atomic emission spectroscopy (Model: ARL 3520). The system was calibrated for simultaneous analyses of Cr and Ni using spectroscopic grade standards. Appropriate emission lines having maximum intensity were selected for analyses and accuracy of the system was found to be within 1%. Repeatability of the measurements was checked and relative standard deviation was found to be less than 1%.

3. Results and discussion

3.1. Microstructure of unexposed and exposed Alloy 690 coupons

Representative BSE images showing the surface morphology of unexposed and exposed (384 h) Alloy 690 coupons are given in Fig. 2(a)–(d). It is observed that as received Alloy 690 has more or less clear grain boundaries and contains isolated TiN precipitates, often partially surrounded with Cr carbide (Fig. 2(a)). On exposure to simulated HLW, grain boundaries close to the surface were found to have opened up (Fig. 2(b)–(c)). Widths of grain boundary openings (Fig. 2(c)) appear to increase with increase in exposure time. BSE images of sample cross-sections show that the liquid attack was not restricted to the surface alone; it also affected the bulk close to the surface (Fig. 2(d)). For the present investigation, the extensive intergranular attack is due to HLW chemistry, which includes sulfate and nitrate anions in addition to various other salts. Earlier Was and Rajan [4] reported that the presence of sulfur in solution promotes intergranular cracking within Ni–Cr–Fe alloys. To find the alloy chemistry close to open grain boundaries, spot X-ray analyses were done at several points. These data are compared with those obtained from unaffected grain boundary regions of respective Alloy 690 coupons. Representative data obtained from Alloy 690 coupon exposed for 384 h are shown in Fig. 3. It is observed that close to open grain boundaries Cr Kα intensity decreased along with those for Ni Kα and Fe Kα as compared to unaffected grain boundaries. This indicates that Ni, Cr and Fe get leached out from Alloy 690 surface upon exposure to HLW. Cr/Ni intensity ratio is found to decrease from ~0.60 (unexposed surface) to

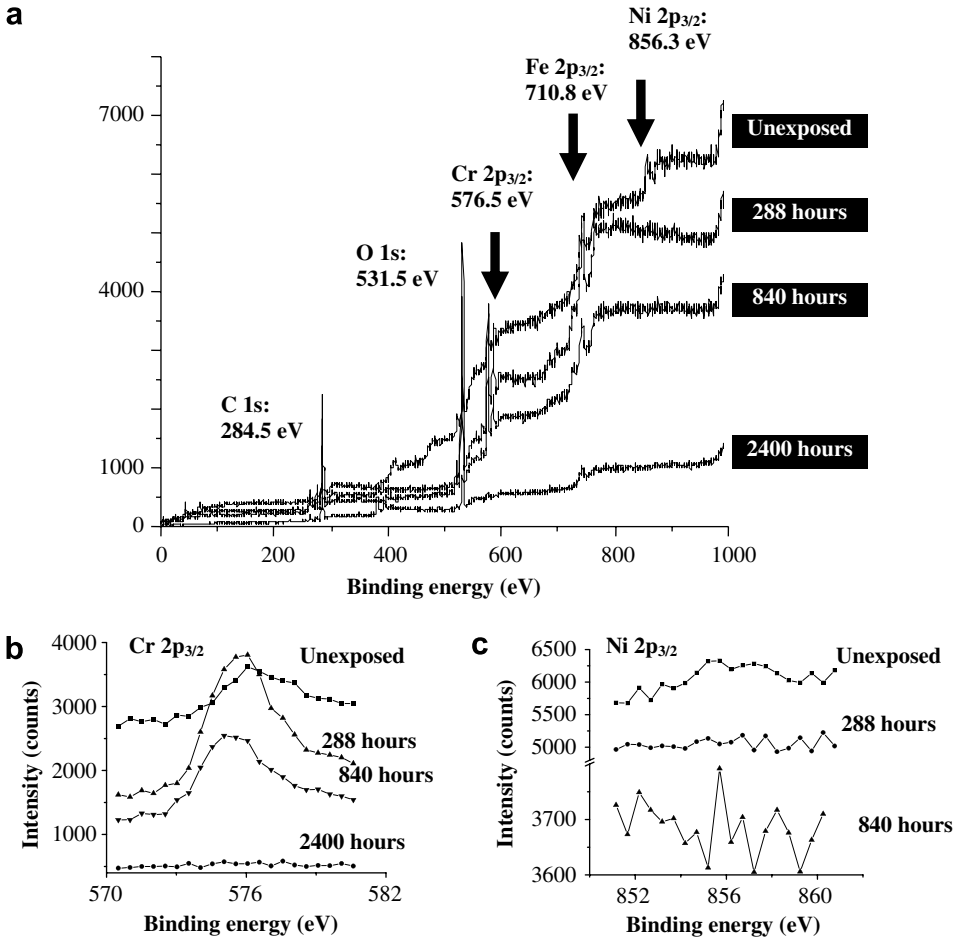

Fig. 4. XPS spectra obtained for unexposed Alloy 690 coupon and the ones exposed to simulated HLW for 288, 840 and 2400 h. (b)–(c) Cr $2p_{3/2}$ and Ni $2p_{3/2}$ spectra showing the changes in peak positions with exposure time.

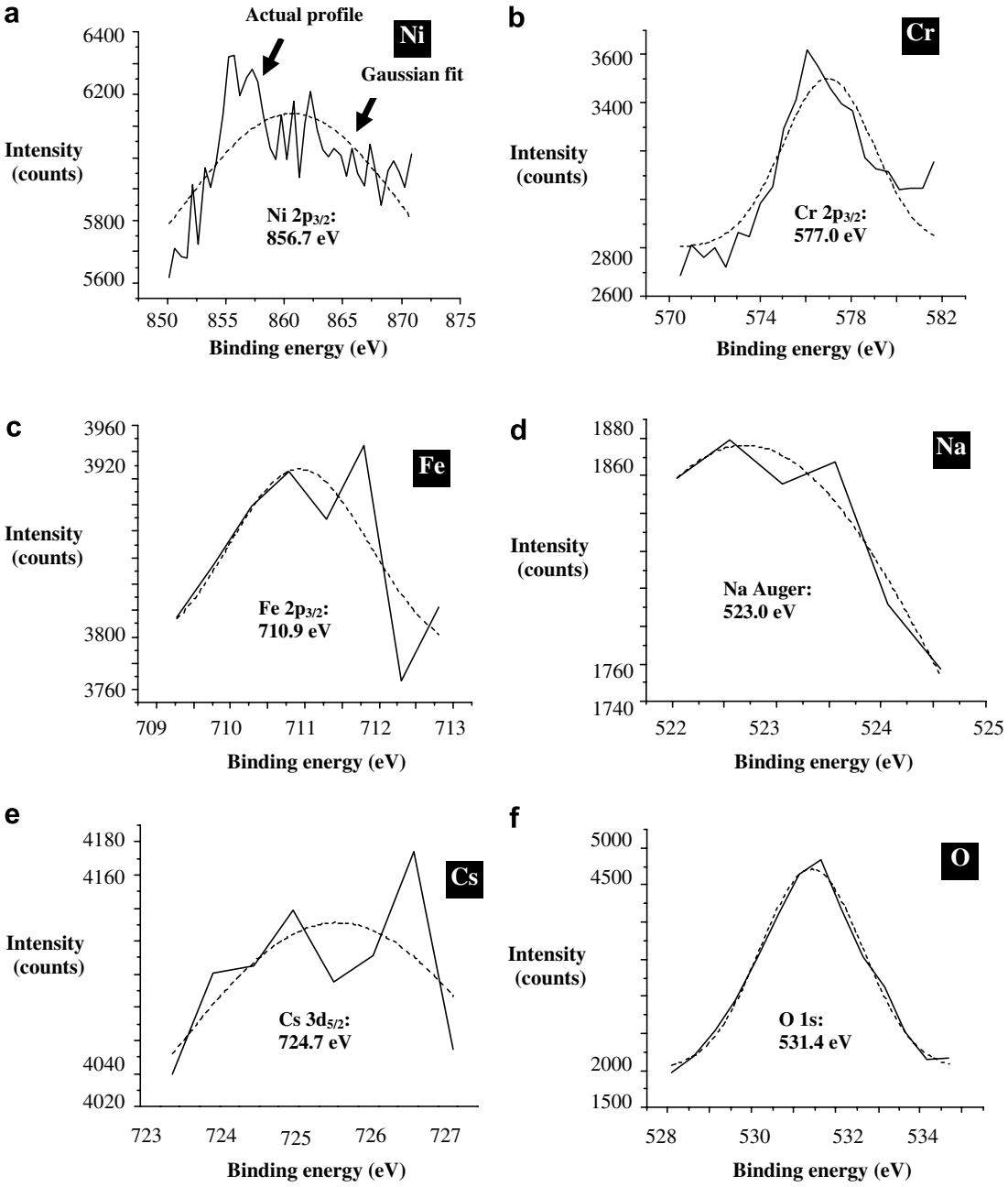

Fig. 5. XPS spectra (for 288 h exposed sample) showing major peak positions.

~0.50 (exposed surface), which indicates preferential loss of Cr with respect to Ni. Gradual increase in Cr and Ni concentrations within HLW leachates with increase in exposure time also supports this observation (discussed later). Earlier, Kai et al. [5] reported cause and effect relationship between Cr depletion and intergranular attacks for Alloy 690. Thus with increase in Cr loss from Alloy 690, the intergranular attack is also likely to be more intensive.

To identify the chemistry of surface layer, XPS analyses of all the samples including as-received unexposed mill annealed sample were carried out. Fig. 4(a)–(c) shows the XPS spectra obtained from unexposed sample and test coupons exposed to HLW for 288, 840 and 2400 h. For unexposed sample, XPS spectra were recorded for $2p_{3/2}$ levels of Ni, Cr and Fe and 1s levels of O and C. The $Ni2p_{3/2}$ XPS peak occurs at a binding energy of 857.0 eV that is higher than that for elemental Ni (852.7 eV) and matches well with corresponding peak in Ni_2O_3. Similarly, $Cr2p_{3/2}$ (576.8 eV) and $Fe2p_{3/2}$ (710.9 eV) peaks also corroborate well with respective peak positions for Cr_2O_3 and Fe_2O_3. Corresponding peak positions for elemental Cr and Fe are at 574.3 eV and 706.7 eV, respectively. For O, 1s level XPS peak occurs at 531.5 eV and it matches with peak positions corresponding to metal oxides. Thus it can be said that Alloy 690 process pot develops a mixed oxide coating of Ni_2O_3–Cr_2O_3–Fe_2O_3 due to atmospheric exposure before

Table 3
Representative data showing compositional evolution of HLW leachate upon exposure to Alloy 690 for different time lengths along with Cr- and Ni-based leach rates

Exposure time (h)	Cr (g/100 ml)	Ni (g/100 ml)	Cr leach rates ($g\,m^{-2}\,d^{-1}$)	Ni leach rates ($g\,m^{-2}\,d^{-1}$)
0 (simulated waste)	0.0580	0.0740	–	–
96	0.0649	0.0783	0.329	0.09
840	0.0804	0.1092	1.067	0.75
1200	0.0840	0.1271	1.238	1.13
1800	0.0886	0.1732	1.457	2.11
2400	0.0919	0.1928	1.610	2.52

its actual plant scale usage. C 1s level peak (284.5 eV) matches well with that of elemental C and its presence indicates marginal C contamination.

XPS spectra obtained for Alloy 690 coupon exposed to HLW for 288 h are shown in Fig. 5(a)–(f). Detailed analysis of the spectrum suggests the presence of a composite surface layer containing Ni, Cr, Fe along with Na, Cs, S and O. The Ni-, Cr- and Fe XPS spectrum with Gaussian fit shows (Fig. 5(a)–(c)) that Ni $2p_{3/2}$, Cr $2p_{3/2}$ and Fe $2p_{3/2}$ peaks occur at 856.7 eV, 577.0 eV and 710.9 eV, respectively, which matches well with corresponding peak positions for Ni_2O_3, Cr_2O_3 and Fe_2O_3. Na auger peak is found to occur at 523.0 eV position (Fig. 5(d)). Besides these, Cs $3d_{5/2}$ peak is also observed whose peak position (724.7 eV, Fig. 5(e)) corroborates well with that in Cs_2SO_4. O 1s XPS peak is found to be at 531.4 eV (Fig. 5(f)), which indicates the possibility of its existence as both metal oxides and sulfates. Combining all these XPS data, it becomes clear that the interaction of Alloy 690 with sulfate containing HLW results in the formation of mixed oxide (Ni_2O_3–Cr_2O_3–Fe_2O_3) layer on alloy surface that also contains Na- and Cs sulfate precipitates. In separate investigations, Dutta et al. [6] and Marcus and Grimal [7], however, reported the formation of mixed oxide–hydroxide surface films on Alloy 690 and other Ni–Cr–Fe alloys. Such variation in surface layer chemistry is due to the difference in leachate compositions and experimental conditions. Significant reductions of Ni $2p_{3/2}$, Cr $2p_{3/2}$, Fe $2p_{3/2}$ peak intensities and increase in O 1s peak intensity for exposed coupons with respect to unexposed sample indicate continuous surface layer.

Table 4
Incremental corrosion rate calculated on weight loss basis

Serial number	Exposure period (h)	Initial weight of coupon (g)	Weight loss (g)
1	96	1.5412	0.0044
2	192	1.6038	0.0075
3	288	1.6276	0.0101
4	384	1.6431	0.0104
5	840	1.4954	0.0228
6	1200	1.5678	0.0442
7	1800	1.6269	0.0819
8	2400	1.5853	0.1204

3.2. Corrosion rate estimation

Compositional analyses of leachate after the completion of each experiment were carried out. It is observed that Cr and Ni concentrations within HLW gradually increased with increase in time of exposure (Table 3). This suggests that despite the formation of surface film, Cr and Ni get continuously leached out from Alloy 690 with time. Thus, the surface film formed on Alloy 690 is either not capable of stopping elemental diffusion or has lot of openings within it. To determine the time dependence of material loss (Table 4), differences in initial and final weights of the coupons are plotted against time (Fig. 6). The best fit line gives good correlation factor ($r^2 = 0.97$) and defines the time dependence material loss relationship by the following linear equation:

$$\Delta w\ (\text{material loss}) = -7.05 + 0.05\ t. \quad (1)$$

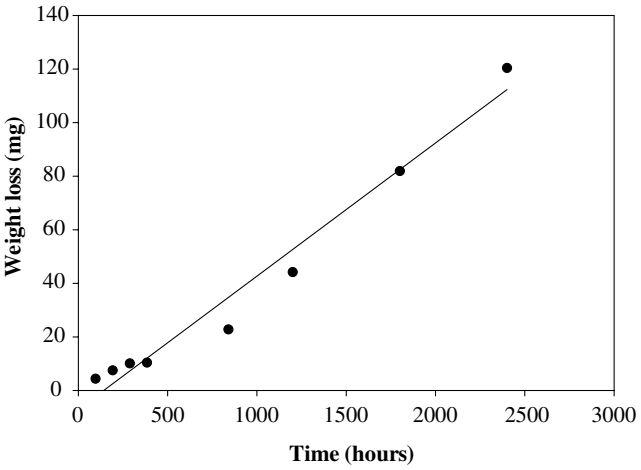

Fig. 6. Time dependence of material weight loss.

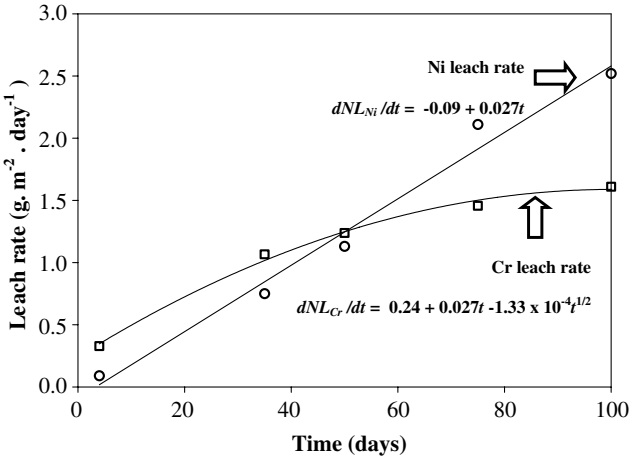

Fig. 7. Time dependence of Ni- and Cr-based leach rates.

Time dependence of material loss has also been calculated following the relationship:

$$(\text{mpy}) = 534 \cdot \Delta w/d \cdot a, \quad (2)$$

where mpy is mills per year, Δw is weight loss (mg), d is density (g/cm^3), a is area (sq. in), and t is time (h).

The value obtained for the coupon exposed to HLW for maximum period, i.e. 2400 h, is 3.66 mpy (assuming density = 8.19 g/cm^3) .

Chemical durability of Alloy 690 coupons has been further assessed by calculating elemental leach rate (g m^{-2} d^{-1}) for Cr and Ni, using the following relationship:

$$\mathrm{dNL}_i/\mathrm{d}t = \Delta/x_i.a.t, \quad (3)$$

where $\mathrm{dNL_i}/\mathrm{d}t$ is leach rate, Δw is w mass loss of element i (g), x_i is mass fraction of i in Alloy 690, a is surface area (m^2) and t is time (day). Cr and Ni leach rates obtained for the 2400 h exposed coupon are 1.61 g m^{-2} d^{-1} and 2.52 g m^{-2} d^{-1}, respectively (Table 3). To find out the time dependence of Ni and Cr leach rates, data were plotted against time (Fig. 7). It is observed that Ni leach rates follow a linear kinetics ($r^2 = 0.98$) of the following type:

$$\mathrm{dNL_{Ni}}/\mathrm{d}t \text{ (leach rate)} = -0.09 + 0.027t. \quad (4)$$

In the case of Cr based leach rates, a non-linear relationship ($r^2 = 0.99$) of the following type is observed:

$$\mathrm{dNL_{Cr}}/\mathrm{d}t \text{ (leach rate)} = 0.241 + 0.027t\text{–}1.33 \times 10^{-4} t^{1/2}. \quad (5)$$

Thus, it is clear from Fig. 7 that Ni leaching from Alloy 690 by hot HLW kept continuing with almost the same rate even after 100 days exposure, whereas in the case of Cr, the leach rates gradually slowed down after 40 days. In other words, growth of the mixed oxide surface layer on Alloy 690 did not affect Ni leaching but reduced Cr release after a certain time.

4. Conclusion

The present experimental studies show that prolonged exposure of Alloy 690 process pot to sulfate containing HLW imposes physical and chemical changes within the material. These include (a) depletion of Cr from the alloy at the interface, (b) intergranular attack and (c) building up of Cr_2O_3–Ni_2O_3–Fe_2O_3 mixed oxide surface layer containing Na and Cs sulfate precipitates. The extents of these alterations have been determined via different routes and in each case they are found to increase with increase in exposure time. Time dependence of material loss from Alloy 690 is found to follow a linear relationship of the type Δw (material loss) $= -7.05 + 0.05t$. Corrosion rate calculated for the coupon exposed to HLW for 2400 h is 3.66 mpy. Materials degradation has been assessed on the basis of Cr and Ni leach rates also. It is found that at the end of 2400 h exposure, the Cr and Ni leach rates are 1.61 g m^{-2} d^{-1} and 2.52 g m^{-2} d^{-1}, respectively. Ni leach rates followed a linear time dependence relationship of the type $\mathrm{dNL_{Ni}}/\mathrm{d}t$ (leach rate) $= -0.09 + 0.027t$. On the other hand, Cr leach rates obeyed a non-linear relationship of the type $\mathrm{dNL_{Cr}}/\mathrm{d}t$ (leach rate) $= 0.241 + 0.027t - 1.33 \times 10^{-4} t^{1/2}$. In actual plant scale operations, these time-based relationships may change significantly as the harsh service conditions within process pot that produce during vitrification of sulfate containing HLW were not considered here.

Acknowledgements

The authors are grateful to Dr. S. Banerjee, Director, Bhabha Atomic Research Centre and Shri S.D. Misra, Director, Nuclear Recycle Group for their keen interests in the work. Analytical help received from Ms. Valsala, Waste Management Division and Ms. N. Mithal, Technical Physics and Prototype Engineering Division are thankfully acknowledged.

References

[1] C.P. Kaushik, R.K. Mishra, P. Sengupta, Amar Kumar, D. Das, G.B. Kale, K. Raj, J. Nucl. Mater. 358 (2006) 129.
[2] K. Raj, in: Proceedings Nuclear fuel cycle technologies: closing the fuel cycle, Indian Nuclear Society, 2003.
[3] R. Do Quang, P. Mougnard, C. Ladirat, A. Prod'homme, in: Environmental issues and waste management technologies in the ceramic and nuclear industries IX, vol. 155, 2004, p. 197.
[4] G.S. Was, V.B. Rajan, Metall. Trans. A 18A (1987) 1313.
[5] J.J. Kai, G.P. Yu, C.H. Tsai, M.N. Liu, S.C. Yao, Metall. Trans. A 20A (1989) 2057.
[6] R.S. Dutta, A. Lobo, R. Purandare, S.K. Kulkarni, G.K. Dey, Metall. Trans. A 33A (2002) 1437.
[7] P. Marcus, J.M. Grimal, Corr. Sci. 33 (1992) 805.